

1 Recovery of stratigraphic data with associated uncertainties from drillhole databases using litho2strat
2 1.0

3 Vitaliy Ogarko^{1,2} and Mark Jessell^{1,2}

4 ¹Centre for Exploration Targeting (School of Earth Sciences), The University of Western Australia,
5 Crawley, 6009 WA, Australia

6 ²Mineral Exploration Cooperative Research Centre, The University of Western Australia, Crawley,
7 6009 WA, Australia

8 CorrespondenceCorrespondance: Vitaliy Ogarko (vitaliy.ogarko@uwa.edu.au)

9

10

Formatted: French (France)

Formatted: French (France)

Formatted: French (France)

Formatted: French (France)

Field Code Changed

11 Abstract

12

13 Australian commonwealth, state and territory geological surveys possess information on over 3 million
14 drillhole logs. In addition to mineral exploration drilling, extensive drillhole datasets exist from oil and
15 gas exploration and hydrogeological studies. There are many more wells drilled in the search for oil and
16 shallower holes related to hydrogeology. Other countries no doubt have similar data holdings.
17 Together these legacy drillhole datasets have the potential to significantly improve our subsurface data
18 coverage but have limited use as constraints on regional 3D geological models as many if not most drill
19 logs lack stratigraphic information, containing only lithological descriptions. Together these legacy
20 drillhole datasets have the potential to significantly improve our subsurface data coverage but have
21 limited use as constraints on regional 3D geological models as many if not most drill logs lack
22 stratigraphic information.

Formatted: Justified

23 This study develops open-source codes and methodologies for stratigraphy recovery (determining the
24 ordered sequence of stratigraphic units) from drillhole lithological data by introducing a search
25 algorithm that systematically explores all geologically plausible stratigraphic orderings for individual
26 drillholes, combined with a solution correlation algorithm that compares the topological relationships
27 of stratigraphic units across multiple drillholes to identify geologically consistent solutions and reduce
28 uncertainty. The algorithms combine constraints from lithological descriptions with stratigraphic
29 relationships automatically derived from regional maps. In addition, the method quantifies uncertainty
30 by generating multiple plausible stratigraphic interpretations, providing critical insights for resource
31 estimation, scenario analysis, and data acquisition strategies.

32 This study develops open source codes and methodologies for stratigraphy recovery from drillhole
33 databases by introducing a correlation algorithm that integrates data from multiple drillholes. The
34 algorithms combine constraints from lithological descriptions, with stratigraphic relationships
35 automatically derived from regional maps. In addition, by integrating uncertainty quantification and
36 presenting multiple geological hypotheses, the resulting stratigraphical description provide critical
37 insights for resource estimation, scenario analysis, and data acquisition strategies.

38 The application of our method to a dataset of 52 drillholes from South Australia demonstrated its
39 ability to make useful predictions of stratigraphic solutions and quantifying associated uncertainties.
40 These results not only validate our approach but also highlight opportunities to refine current
41 stratigraphic descriptions and provide a valuable new source for regional 3D geological modelling.

42

43

44 1. Introduction

45

46 Drillhole data serves as a fundamental constraint for subsurface geological exploration and 3D
47 geological modelling, offering direct insights into lithological and hence stratigraphic features
48 (Wellmann & Caumon, 2018). However, the inherent sparsity of such data, coupled with challenges
49 posed by legacy datasets maintained by industry and Geological Survey Organizations (GSOs), often
50 hinders comprehensive geological understanding and modelling (Jessell et al., 2010; Pakyuz-Charrier
51 et al., 2018). GSOs' databases typically contain complexly coded lithological information but limited
52 stratigraphic data, GSOs' databases typically contain lithological information as unstructured text
53 descriptions (e.g., 'sandy limestone with minor shale') but rarely include stratigraphic unit
54 assignments. This creates a critical gap in the data needed for accurate and meaningful
55 geological predictions (Hartmann & Moosdorf, 2012).

56 Geological modelling plays a crucial role in understanding subsurface structures and processes,
57 providing a foundation for various applications in earth sciences (M. Jessell et al., 2014). Such
58 modelling commonly relies on datasets such as borehole data, geophysical data, and mapping data.
59 From Among these, borehole data provide the most accurate insights into subsurface geology and
60 stratigraphy (Guo et al., 2022). The models generated through geological modelling can serve dual
61 purposes: they can be directly employed for geological interpretations, such as identifying fault
62 systems, and mineral deposits (Alvarado-Neves et al., 2024; Vollgger et al., 2015), or they can be
63 integrated as constraints in methodologies that use a prior 3D model, such as geophysical inversions
64 (Giraud et al., 2017; Martin et al., 2024; Ogarko et al., 2021; Tarantola, 2005) and hydrogeological
65 forward modelling (D'Affonseca et al., 2020). By incorporating geological models into geophysical
66 inversion, it is possible to refine the interpretation of subsurface properties and achieve greater
67 accuracy in representing complex geological environments.

68 Modern drillhole measurement techniques primarily focus on chemical, mineralogical and lithological
69 characterization, whereas the fundamental categorical unit of regional 3D geological models is defined
70 by its stratigraphy (Calcagno et al., 2008; Caumon et al., 2009; Mallet, 2002). This discrepancy
71 underscores the need for innovative approaches to recover and integrate stratigraphic information
72 from existing datasets. Recent advancements in automation, particularly through machine learning
73 and natural language processing, have demonstrated significant potential in addressing these
74 challenges by standardizing and extracting lithological and stratigraphic data at scale (Guo et al., 2024;
75 Joshi et al., 2021; Schetselaar & Lemieux, 2012).

76 Modern drillhole measurement techniques primarily focus on chemical, mineralogical and lithological
77 characterization, whereas the fundamental categorical unit of regional 3D geological models is defined
78 by stratigraphy (Calcagno et al., 2008; Caumon et al., 2009; Mallet, 2002). This discrepancy
79 underscores the need for innovative approaches to recover and integrate stratigraphic information
80 from existing datasets.

81 Recent advancements in automation have made significant progress in processing drillhole data,
82 though most address different aspects of the problem than stratigraphic recovery. Data
83 standardization tools like dh2loop (Joshi et al., 2021) extract and harmonize lithological descriptions
84 from unstructured text using thesauri and fuzzy string matching, providing essential preprocessing for
85 downstream analysis. Pattern recognition methods (Schetselaar & Lemieux, 2012) can identify
86 lithostratigraphic markers and contacts within drill logs, helping to detect boundaries between units.
87 Machine learning approaches for 3D geological modeling (Guo et al., 2024) can interpolate between
88 drillholes to create subsurface models, but typically require pre-interpreted stratigraphic data as input.

89 While these methods provide valuable components of the workflow, none directly address the
90 fundamental challenge of transforming lithological descriptions into stratigraphic interpretations with
91 quantified uncertainties.

92 Existing automated interpretation methods primarily work with different data types than those
93 available in legacy drillhole databases. Geophysics-based methods (Wu & Nyland, 1987; Fullagar et al.,
94 2004; Silversides et al., 2015) leverage distinctive signatures in gamma, resistivity, or other wireline
95 logs to predict stratigraphic units, but require geophysical data that are absent from most legacy
96 drillholes. Geochemical and spectral approaches (Hill & Uvarova, 2018) use XRF scanning or
97 hyperspectral measurements to identify geological boundaries with high precision, but depend on
98 expensive data acquisition unavailable in historical datasets. Hybrid machine learning methods, such
99 as those applied in the Pilbara iron ore deposits (Wedge et al., 2019), combine lithology with assays
100 and geophysics but require extensive pre-interpreted drillhole datasets for training, limiting their
101 application in greenfield exploration areas. These approaches do not address the fundamental
102 challenge faced by geological surveys worldwide: millions of legacy drillholes contain only lithological
103 descriptions but lack both stratigraphic interpretations and the geophysical logs required by current
104 automated methods.

105 To address these challenges, we formulate the problem of stratigraphic recovery from drillhole
106 databases as follows. The input to our methodology consists of: (1) legacy drillhole databases
107 containing lithological descriptions (e.g., "sandstone", "siltstone", "dolomite") at various depth
108 intervals, typically without stratigraphic labels; (2) regional geological maps that define stratigraphic
109 unit boundaries and their spatial relationships; and (3) topological constraints that specify which
110 stratigraphic units can be in contact based on their known relative ages and depositional sequences.

111 The output comprises: (1) multiple plausible stratigraphic solutions, where each solution provides unit
112 assignments for all depth intervals in the drillholes; (2) their ranking by geological likelihood; and (3)
113 quantified uncertainties for these interpretations. The objective is threefold: first, to systematically
114 transform lithological descriptions into stratigraphic interpretations by testing all geologically plausible
115 orderings of stratigraphic units that are consistent with the observed lithologies; second, to quantify
116 the uncertainty inherent in these interpretations given that multiple stratigraphic units may share
117 similar lithological characteristics; and third, to establish correlations between multiple drillholes to
118 reduce uncertainty and improve the reliability of stratigraphic assignments across a region. This
119 transformation is essential because regional 3D geological models are fundamentally organized by
120 stratigraphy rather than lithology, yet the majority of legacy drillhole data lack stratigraphic labels.

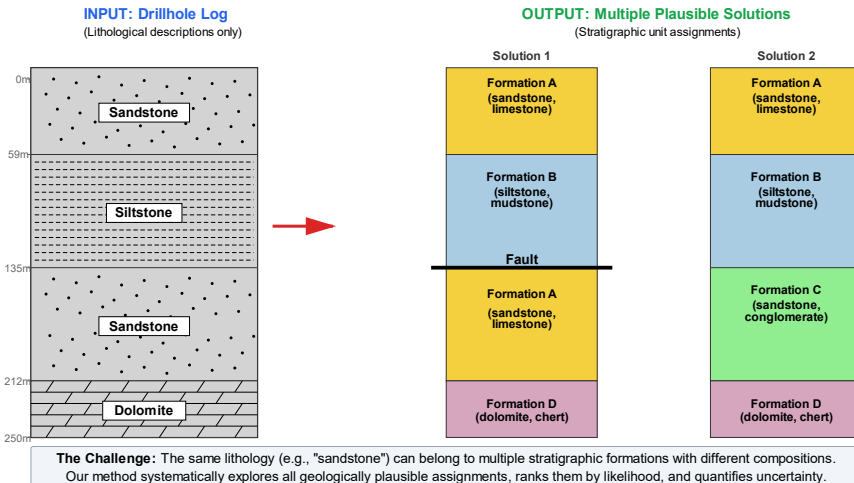
121 Figure 1 illustrates this challenge with a simplified example: a drillhole log with four lithological
122 intervals (sandstone, siltstone, sandstone, dolomite) could correspond to multiple stratigraphic
123 interpretations. The two sandstone intervals might represent the same formation repeated by faulting,
124 or they could belong to different formations with similar but distinct lithological compositions. Without
125 additional constraints, both interpretations are geologically plausible, highlighting the inherent
126 ambiguity in stratigraphic assignment from lithological data alone.

Formatted: Font: Not Bold

Formatted: Font: Not Bold

Formatted: Font: Not Bold

The Challenge of Stratigraphic Interpretation from Lithological Data



127

128 [Figure 1: Schematic illustration of the stratigraphic interpretation problem. A drillhole log containing](#) [only lithological descriptions \(left\)](#) [can yield multiple plausible stratigraphic solutions \(right\)](#) [because the same lithology may occur in different stratigraphic formations with varying compositions.](#)

Formatted: Font: Not Bold

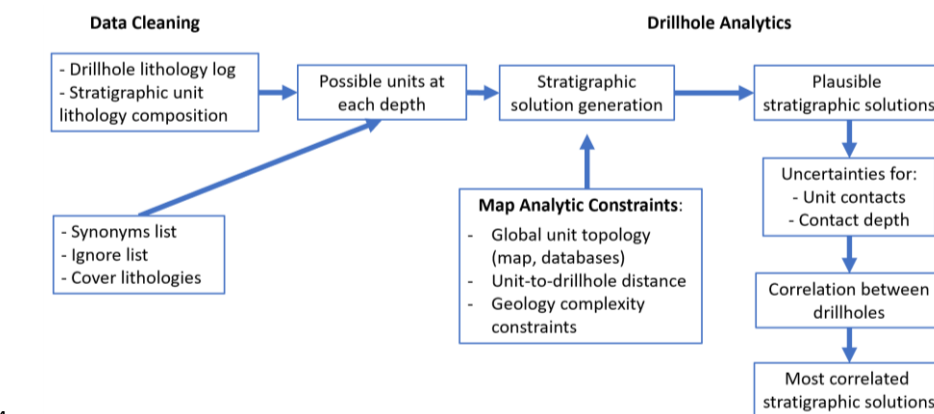
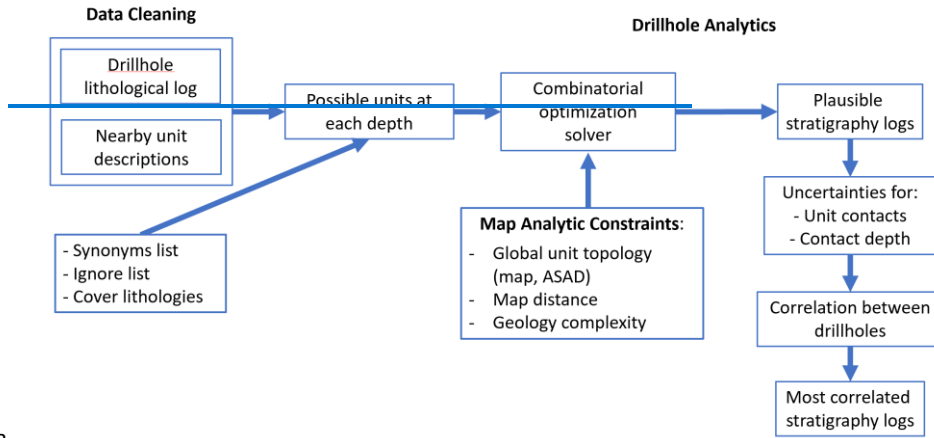
Formatted: Left

131 [This study develops open-source codes and methodologies for stratigraphy recovery from drillhole](#)
 132 [databases by introducing a correlation algorithm that integrates data from multiple drillholes, we](#)
 133 [enhanced the robustness and reliability of stratigraphic interpretations. By integrating uncertainty](#)
 134 [quantification and presenting multiple geological hypotheses, the resulting stratigraphical description](#)
 135 [provide critical insights for resource estimation, scenario analysis, and data acquisition strategies. The](#)
 136 [application of our method to a dataset of 52 drillholes from South Australia demonstrated its ability to](#)
 137 [make useful predictions of stratigraphic solutions and quantifying associated uncertainties. These](#)
 138 [results not only validate our approach but also highlight opportunities to refine current stratigraphic](#)
 139 [descriptions, improving workflow accessibility and paving the way for more effective geological](#)
 140 [assessments and decision-making processes.](#)

141 [This study develops open-source codes and methodologies for stratigraphy recovery from drillhole](#)
 142 [lithological data through a two-stage approach. First, we introduce a branch-and-prune search](#)
 143 [algorithm that systematically explores all geologically plausible stratigraphic orderings for individual](#)
 144 [drillholes. Second, we apply a solution correlation algorithm that integrates information from multiple](#)
 145 [drillholes by comparing topological relationships of stratigraphic units, thereby enhancing the](#)
 146 [robustness and reliability of interpretations. The method quantifies uncertainty by generating multiple](#)
 147 [plausible stratigraphic interpretations, providing critical insights for resource estimation, scenario](#)
 148 [analysis, and data acquisition strategies. We apply our method to a dataset of 52 drillholes from South](#)
 149 [Australia to demonstrate its practical application and validate its performance against existing](#)
 150 [stratigraphic interpretations.](#)

151 2. Methodology

152 2.1 2.1 Workflow



155 Figure 24: The different stages of the analysis.

156 The workflow shown in Fig. 24 consists of three key steps grouped into three main tasks: Data
 157 Cleaning (using the dh2loop code), Map Analytic Constraints (using map2modelloop and custom
 158 codes developed for this project) and Drillhole Analytics (using the litho2strat code developed for
 159 this project).

160

161 2.1.1 Data Cleaning

162 Prior to analysing the drillhole data we went through a number of automated data cleaning and
 163 harmonisation steps.

164 a) Harmonisation of drillhole lithology descriptions using the dh2loop code described in (Joshi et
 165 al., 2021) (code available here: <https://github.com/Loop3D/dh2loop>) This enables us to

Formatted: Outline numbered + Level: 2 + Numbering Style: 1, 2, 3, ... + Start at: 1 + Alignment: Left + Aligned at: 0 cm + Indent at: 0.81 cm

166 produce a standardised lithological description for multiple drillholes in a region, regardless of
167 their provenance. This includes the use of a synonym list (“granite” vs “granitoid”), and ignore
168 list (e.g. “fault”) together with a list of cover lithology terms (e.g. “saprolite”) that enables us
169 to simplify the list of terms and exclude irrelevant information.

170

171 b) Harmonisation of lithological descriptions for formations described in the geological map of
172 the target area. This ensures that the same terminology is used for borehole lithological
173 descriptions and map lithologies.

174 Together steps a [and](#) b provide a list of possible units at each depth down a drill hole.

175

176 2.1.2 Map Analytic Constraints

177 a) Calculation of the distance between each polygon in a map and the target borehole. A custom
178 Python script was developed. This information can be used as a guide to the likelihood that a
179 drillhole would intersect a given unit.

180 b) We then used the [map2modelloop](#) engine (M. Jessell et al., 2021) (code available here:
181 https://github.com/Loop3D/map2model_cpp—) to
182 extract the topological relationships between the surface expression of stratigraphic different
183 units. This would later be used to assess the likelihood that two units would be in contact in
184 the drillhole.

185

186 [The map2model engine extracts topological relationships between stratigraphic units,
187 including both normal depositional contacts and fault contacts, as both types of juxtaposition
188 may be encountered in drillhole data.](#)

189

190 Unit connectivity information can also be obtained from the Australian Stratigraphic Units
191 Database (ASUD) as well as from various published reports containing stratigraphic data. The
192 ASUD serves as a comprehensive repository of geological information, providing valuable
193 insights into the relationships between different stratigraphic units across Australia.
194 Additionally, numerous geological surveys and research studies offer stratigraphic data that
195 can further enrich our understanding of unit connectivity. [By leveraging this information, we
196 can enhance our stratigraphic models, improves the accuracy of correlations between
197 drillholes, and facilitates a deeper understanding of the geological framework in specific
198 regions.](#)

199

200

201 These two steps allow us to capture information on the spatial and topological relationships
202 between the mapped units.

203

204 2.1.3 Drillhole Analytics

205 a) [In this stage of the analysis, we developed a new code called litho2strat \(code available here:
206 <https://github.com/Loop3D/litho2strat>; Ogarko et al., 2025\). The information about code
207 design is detailed in Section 2.4. The code uses a combinatorial optimisation solver as
208 follows:](#)

209 — We employed a Branch and Bound algorithm, which is a powerful method for solving
210 optimization problems (Land & Doig, 1960). This approach systematically enumerates all
211 potential candidate solutions by exploring the state space.

212 — New branches could be added while traversing the drillhole log from top to bottom, using a
213 list of possible units at each depth down a drill hole and a unit topological relationship.

214 — We applied bounds by adding solution constraints. The branch is discarded if it does not
215 satisfy the constraints. The types of constraints we apply are discussed in Section 2.2.

216 — In the end, we could obtain a plausible set of solutions fitting the data and satisfying the
217 constraints. This strategy not only ensures a thorough exploration of the solution space but
218 also optimizes efficiency by eliminating unnecessary computations, ultimately leading to a
219 more effective and streamlined search process.

220 — Finally, we calculated the uncertainties directly from the whole set of solutions.

221 In this stage, we employ the litho2strat code to establish correlations between drillholes, which
222 helps to reduce uncertainty in the calculated set of plausible stratigraphic solutions. The
223 correlated solution scores are assigned based on overall uncertainty, with solutions receiving the
224 highest scores selected as the most plausible options. For further details on the correlation
225 algorithm utilized, please refer to Section 2.3.

226 In this stage, we employ the litho2strat code to generate plausible stratigraphic solutions that fit
227 the observed lithological data while satisfying all geological constraints (code available here:
228 <https://github.com/Loop3D/litho2strat>; Ogarko et al., 2025). The algorithm uses a recursive
229 branch and prune approach to efficiently explore the solution space, eliminating geologically
230 implausible pathways early in the search process (see Section 2.2 for detailed algorithm
231 description). This strategy not only ensures thorough exploration of viable stratigraphic orderings
232 but also optimizes computational efficiency by avoiding unnecessary enumeration of invalid
233 solutions.

234 From the complete ensemble of plausible solutions obtained for each drillhole, we calculate
235 uncertainties that quantify the confidence in different stratigraphic interpretations. Solutions are
236 scored based on the probability of unit contacts within the local solution ensemble, providing a
237 ranking of stratigraphic hypotheses from most to least likely.

238 To further reduce uncertainty and improve solution reliability, we implement a correlation
239 algorithm that leverages information from multiple neighboring drillholes simultaneously (see
240 Section 2.5 for correlation algorithm details). By comparing the topological relationships of
241 stratigraphic units across drillholes, the correlation process identifies solutions that are
242 geologically consistent across the broader area. Correlated solution scores integrate both local
243 evidence from individual drillholes and regional consistency with neighboring holes, with
244 solutions receiving the highest correlated scores selected as the most plausible stratigraphic
245 interpretations.

246

247 [2.2 Stratigraphic solution generation](#)

Formatted: Outline numbered + Level: 2 + Numbering
Style: 1, 2, 3, ... + Start at: 1 + Alignment: Left + Aligned
at: 0 cm + Indent at: 0.81 cm

Formatted: Font: Not Bold

249 [The litho2strat algorithm operates through a hierarchical search strategy that systematically explores](#)
250 [the space of possible stratigraphic orderings \(solutions\) while pruning geologically implausible](#)
251 [solutions. The algorithm can be formally described as follows:](#)

252 [**Input:**](#)

253 • [L = {l₁, l₂, ..., l_n} : sequence of lithologies observed at depths d₁ < d₂ < ... < d_n](#)

254 • [U = {u₁, u₂, ..., u_m} : set of m candidate stratigraphic units, each defined by its constituent](#)
255 [lithologies](#)

256 • [C : set of geological constraints \(distance, connectivity, complexity\)](#)

257 • [Γ : global unit connectivity graph derived from geological maps and stratigraphic databases](#)

258 [**Output:**](#)

259 • [S = {s₁, s₂, ..., s_k} : set of k plausible stratigraphic solutions](#)

260 • [P\(s_i\) : probability distribution over solutions](#)

261 • [G_h : local connectivity graph for drillhole h, derived from all solutions for this drillhole](#)

262 [**Algorithm Steps:**](#)

263 [**1. Unit Matching Phase:** For each lithology l_i at depth d_i, identify the subset of compatible units:](#)

$$M(l_i) = \{u_j \in U \mid \text{lithology}(u_j) \text{ matches } l_i \text{ AND satisfies constraints } C\}$$

265 [**2. Recursive Branch and Prune Exploration:** The algorithm recursively builds the solution space from](#)
266 [shallow to deep depth intervals. Starting from the surface, partial solutions are extended one depth](#)
267 [level at a time by considering candidate units that match the observed lithology. The algorithm](#)
268 [generates a new branch for candidate unit u_i only when all of the following conditions are satisfied:](#)

269 • [The unit u_i matches the observed lithology at the current depth](#)

270 • [The extended solution satisfies all constraints in C \(distance, occurrence, contact complexity\)](#)

271 • [For the last unit u_k in the partial solution, the edge \(u_k, u_i\) exists in the global connectivity](#)
272 [graph Γ](#)

273 [Partial solutions that violate any condition are immediately abandoned \(pruned\), preventing](#)
274 [exploration of their extensions. When a partial solution reaches the deepest depth interval, it is](#)
275 [validated and added to the solution set S. This recursive approach with constraint-based pruning](#)
276 [eliminates large portions of the solution space without explicit enumeration.](#)

277 [The algorithm systematically explores all geologically valid solutions through exhaustive search with](#)
278 [constraint-based pruning. While the top-to-bottom traversal order does not affect the completeness](#)
279 [of the final solution set S \(the same valid stratigraphic interpretations would be found regardless of](#)
280 [traversal direction\), it does improve computational efficiency by enabling earlier application of](#)
281 [surface geology constraints and more effective pruning of invalid solution branches.](#)

282 [**3. Local Connectivity Graph Construction:** From the complete set of solutions S obtained for drillhole](#)
283 [h, construct a local connectivity graph G_h where edge weights represent the frequency of unit](#)
284 [contacts across all solutions:](#)

$$w_h(u_i, u_{i+1}) = | \{s \in S : (u_i, u_{i+1}) \text{ adjacent in } s\} | / |S|$$

286 This directed local graph captures the probability of unit contacts based on the ensemble of
287 geologically plausible solutions for drillhole h , where edges represent stratigraphic ordering. Each
288 edge weight represents the fraction of solutions in which the corresponding unit contact appears.
289 Note that G_h is a subgraph of the global connectivity graph Γ , as all solutions for drillhole h must
290 satisfy the global connectivity constraints.

Formatted: Font: Italic

291 **4. Solution Scoring:** For each solution $s_i \in S$, calculate a normalized score based on the local
292 connectivity graph G_h :

$$293 \text{score}(s_i) = \sum_j w_{hj}(u_i, u_{i+1}) / N_i$$

294 where N_i is the number of unit contacts in solution s_i (i.e., $N_i = |s_i| - 1$), and the sum is over all
295 consecutive unit pairs. The normalization by N_i ensures that solutions with different numbers of
296 stratigraphic contacts are directly comparable, preventing bias toward longer or more complex
297 solutions. The score thus represents the average edge probability across all contacts in the solution.

298 **5. Probability Calculation:** Normalize scores to obtain probability distribution:

$$299 P(s_i) = \text{score}(s_i) / \sum_k \text{score}(s_k)$$

300 The efficiency of this approach derives from constraint-based pruning during the recursive
301 exploration. By evaluating both solution constraints C and global connectivity Γ before extending
302 each partial solution, the algorithm eliminates inconsistent paths immediately without exploring
303 their complete extensions. The distinction between the global connectivity graph Γ (used for
304 constraint validation during exploration) and the local connectivity graph G_h (derived from solutions
305 and used for scoring) is crucial: Γ represents *a priori* geological knowledge from maps and databases,
306 while G_h captures the *a posteriori* probability distribution of unit contacts specific to drillhole h given
307 all constraints.

308

309 2.3 2.2 Solution constraints

310

311 For the Branch and Bound (BnB) algorithm, providing efficient constraints (bounds) is crucial for
312 generating geologically plausible stratigraphies and reducing the search space. Without these
313 bounds, the BnB algorithm reverts to exhaustive search, which is less efficient. We utilize two types
314 of solution constraints: the first can be derived from geological maps (as discussed in the 'Map
315 Analytic Constraints' section), while the second is selected by the user based on the expected
316 geological complexity of the area (e.g., the presence of known faults).

317 The specific constraints employed include:

- 318 1. **Distance from the Drillhole to the Unit:** This constraint limits the number of geological units
319 considered in the calculations, ensuring relevance to the drillhole's location.
- 320 2. **Global Unit Connectivity:** This constraint restricts the potential contacts between units,
321 enhancing the accuracy of the stratigraphic model.
- 322 3. **Top Unit Constraint:** Information regarding the top unit can be extracted from geological
323 maps, providing a foundational boundary for the stratigraphy.

Formatted: Outline numbered + Level: 2 + Numbering Style: 1, 2, 3, ... + Start at: 1 + Alignment: Left + Aligned at: 0 cm + Indent at: 0.81 cm

324 4. **Solution Complexity (Occurrence):** This constraint sets a maximum limit on how many times
325 a unit can appear in the final stratigraphy. For example, in the presence of a fault, the same
326 geological unit may appear twice within the same log.

327 5. **Solution Complexity (Contacts):** This constraint defines the maximum number of unit
328 contacts allowed within a continuous sequence of drillhole lithologies. For instance, in a
329 continuous sequence of "sandstone" lithologies, different sandstones may belong to
330 separate geological units.

331 These constraints work together to enhance the efficiency and effectiveness of the BnB
332 algorithm, ensuring that the resulting stratigraphies are both plausible and reflective of the
333 geological context.

334 For the Branch and Prune algorithm described in Section 2.2, providing efficient constraints
335 (collectively denoted as C) is crucial for generating geologically plausible stratigraphies and reducing
336 the search space. Without these constraints, the algorithm would need to exhaustively enumerate all
337 possible unit assignments, which is computationally prohibitive. We utilize two types of solution
338 constraints: the first can be derived from geological maps (as discussed in the 'Map Analytic
339 Constraints' section), while the second is selected by the user based on the expected structural
340 complexity of the area (e.g., the presence of faults, folds, or other features that might cause
341 stratigraphic repetition or disruption).

342 The specific constraints in C include:

343 1. **Distance Constraint:** This constraint limits the number of geological units considered based on
344 their proximity to the drillhole. In this context this is defined as the distance between the drillhole
345 collar and the nearest point on the polygon's boundary in 2D. For drillhole h and candidate unit $u_i \in$
346 U :

347 $d(u_i, h) \leq d_{max}$,

348 where $d(u_i, h)$ is the distance from the nearest outcrop of unit u_i to drillhole h , and d_{max} is the
349 maximum search radius. This ensures relevance to the drillhole's location.

350 2. **Global Unit Connectivity Constraint:** This constraint, enforced through the global connectivity
351 graph Γ , restricts potential contacts between units. For any two consecutive units u_i and u_{i+1} in a
352 solution:

353 $(u_i, u_{i+1}) \in E(\Gamma)$,

354 where $E(\Gamma)$ is the edge set of the global connectivity graph. This ensures that only units known to be
355 stratigraphically adjacent (from map data, databases, or published reports) can be placed in contact,
356 enhancing the geological plausibility of solutions.

357 The edges in the global connectivity graph Γ can be configured as either single-directional or
358 bidirectional depending on the structural complexity of the study area. In structurally simple areas
359 with normal stratigraphic succession, single-directional edges (e.g., $A \rightarrow B$) enforce the expected
360 younging direction (older to younger upward). However, for areas with known structural complexities
361 such as overturned sequences from folding or thrust faulting, bidirectional edges can be used to
362 allow stratigraphic contacts in both normal and reversed orientations. For example, if units A and B
363 can occur in both normal succession (A overlies B) and overturned succession (B overlies A) due to
364 folding, the graph Γ would include a bidirectional edge between them, allowing transitions in both
365 directions ($A \rightarrow B$ and $B \rightarrow A$). This configuration allows the algorithm to exhaustively explore all

Formatted: Indent: Left: 0 cm

Formatted: No bullets or numbering

Formatted: Indent: Left: 0 cm

Formatted: No bullets or numbering

Formatted: Indent: Left: 0 cm

366 structurally valid solutions including those with reversed polarity sequences. The choice of single-
367 directional versus bidirectional edges in Γ is thus a key input that controls whether the algorithm
368 considers only normal superposition or also accommodates structural inversions.

369 **3. Top Unit Constraint:** Information regarding the top unit $utop$ can be extracted from geological
370 maps at the surface location of the drillhole, providing a foundational boundary condition:

371 $s[0] = utop$,

372 where $s[0]$ denotes the shallowest unit in solution s . Note that while the global unit connectivity
373 constraint allows sequences to begin from any node in the connectivity graph, this constraint
374 explicitly specifies the starting node.

375 **4. Occurrence Constraint:** This constraint sets a maximum limit on how many times a unit can appear
376 in a solution, accounting for geological complexity such as faulting or folding. For unit u_i in solution s_i :

377 $count(u_i, s_i) \leq kmax$,

378 where $count(u_i, s_i)$ is the number of times unit u_i appears in s_i . Typically $kmax = 1$ for unfaulted
379 sequences, or $kmax = 2-3$ for faulted terrains where stratigraphic repetition may occur.

380 **5. Contact Complexity Constraint:** For a continuous sequence of identical lithology observations $[l_i, l_{i+1}, \dots, l_{i+m}]$ where all lithologies are the same, this constraint limits the number of distinct
381 stratigraphic units that can be assigned:

383 $| \{u_i : \text{assigned to interval } [i, i+m]\} | \leq cmax$,

384 where $cmax$ is the maximum number of unit contacts allowed within the continuous lithology
385 sequence. This prevents over-interpretation where a thick monotonous lithology (e.g., a 100m
386 sandstone sequence) is artificially divided into an excessive number of stratigraphic units.

387 **6. Stratigraphic Jump Constraint:** To account for incomplete exposure of geological contacts at the
388 surface, we allow the algorithm to "jump" over intermediate units in the global connectivity graph Γ .
389 For a path in Γ such as $A \rightarrow B \rightarrow C$, setting the maximum number of stratigraphic jumps parameter to
390 $jmax$ allows direct contacts between non-adjacent units up to $jmax$ steps apart in the graph. For
391 example, with $jmax=1$, the algorithm can consider both $A \rightarrow B$ and $A \rightarrow C$ as valid contacts, even if $A \rightarrow C$
392 is not explicitly observed in the map data. This addresses the limitation that geological maps provide
393 only a 2D surface expression of 3D geological relationships and may not capture all possible
394 stratigraphic contacts that exist at depth. The constraint is defined as:

395 $d\Gamma(u_i, u_j) \leq jmax + 1$

396 where $d\Gamma(u_i, u_j)$ is the shortest path distance between units u_i and u_j in the connectivity graph Γ , and
397 $jmax$ is the maximum number of allowed jumps (typically $jmax=0$ for strict adherence to observed
398 contacts, or $jmax=1-2$ for more permissive exploration).

399 These constraints in C work together to enhance the efficiency and effectiveness of the Branch and
400 Prune algorithm, ensuring that the resulting stratigraphies are both geologically plausible and
401 computationally tractable. As demonstrated in Section 3, constraint-based pruning reduces the
402 search space by >99% in practical applications, enabling computation of all valid solutions in seconds.

Formatted: No bullets or numbering

Formatted: Indent: Left: 0 cm

Formatted: No bullets or numbering

Formatted: Indent: Left: 0 cm

Formatted: No bullets or numbering

Formatted: Indent: Left: 0 cm

Formatted: Indent: Left: 0 cm

404 2.4 Computational complexity

405

406 The computational complexity of the branch and prune algorithm depends on several key factors:
407 the number of drillholes H , the length of the lithology sequence $|L|$ (i.e., the number of depth
408 intervals), the number of candidate stratigraphic units $|U|$, and critically, the average number of
409 solutions N maintained during the recursive exploration. The algorithm processes each drillhole
410 independently, and for each drillhole, it iterates through all lithologies in L , evaluating potential unit
411 assignments for each active solution.

412 The theoretical time complexity can be expressed as:

413 $O(H \times |L| \times N \times |U|)$

414 where N denotes the average number of solutions maintained during recursive exploration. This is
415 the most variable factor and depends strongly on the geological complexity and the constraints
416 applied.

417 In the unconstrained case, where no geological constraints are imposed, the number of solutions can
418 grow exponentially with the number of lithology changes k in the drillhole log, potentially reaching N
419 $\propto |U|^k$. This leads to a worst-case complexity of $O(H \times |L| \times |U|^{(k+1)})$, which quickly becomes
420 computationally prohibitive for complex stratigraphic sequences.

421 However, the application of geological constraints C - particularly the global unit connectivity
422 constraint enforced through the topology graph Γ - dramatically reduces the solution space. These
423 constraints prune geologically implausible branches early in the recursive exploration, preventing
424 exponential growth of N . In practice, with appropriately chosen constraints, N grows moderately with
425 the number of lithology changes (approximately linearly rather than exponentially), resulting in
426 manageable computational requirements even for complex stratigraphic sequences.

427 The effectiveness of constraint-based pruning in controlling computational cost is demonstrated
428 empirically in Section 3, where we compare the growth of average solution numbers as a function of
429 lithology changes for cases with and without topology constraints.

430

431 2.5 2.3-Solution correlation

432

433

434 We utilize solution correlation analysis to establish relationships between multiple drillholes, serving
435 as a constraint on the plausibility of stratigraphic ordering. This correlation can be applied either to
436 stratigraphy logs or to the topological relationships of units, represented through connectivity
437 graphs.

438 A key challenge in correlating stratigraphy logs is that units at the same depth may not align across
439 different drillholes, mainly due to variations in unit dip and thickness. To address this, we focus on
440 correlation based on topological relationships. Connectivity graphs are constructed for each drillhole
441 using a plausible set of stratigraphic solutions derived from the Branch and Bound (BnB) solver.

442 In these graphs, the edges are weighted by the probability of unit contacts, calculated as the number
443 of solutions that include a specific unit contact divided by the total number of solutions for that

Formatted: Normal

444 drillhole. This approach enhances the accuracy of the correlations, providing a more reliable
445 framework for establishing stratigraphic relationships.

446 We propose the correlation algorithm as follows:

447 I. **Calculate Solution Scores:** For each solution i , compute the solution score $S(i, G_{\text{self}})$ using
448 the connectivity graph from the current drillhole G_{self} . This score is defined as the sum of
449 the edge weights for all solution contacts, indicating the likelihood of the solution within the
450 current drillhole.

451 II. **Calculate External Solution Scores:** For each external drillhole j , calculate the solution scores
452 $S(i, G_{\text{ext}}^j)$ using their respective connectivity graphs. This score reflects the likelihood of the
453 solution for each external drillhole.

454 III. **Build Final Correlated Solution Score:** Construct the final correlated solution score $C(i)$
455 using the following formula:

$$C(i) = \frac{S(i, G_{\text{self}}) + \sum_{j=1}^{N-1} S(i, G_{\text{ext}}^j)}{N}$$

456 This final score represents the overall likelihood of the solution across all drillholes,
457 effectively correlating the current solution with all solutions from the external drillholes
458 based on the topological relationships of the geological units.

459 The final correlated solution score provides a means to assign correlated scores to various solutions,
460 effectively altering their ranking within the overall assessment. This adjustment not only enhances
461 the clarity of which solutions are more viable but also helps to reduce uncertainty associated with
462 those solutions. By refining the evaluation process in this manner, we can achieve a more precise
463 understanding of the relationships between different geological units. By integrating and correlating
464 drillhole data effectively, we ensure that the stratigraphic framework accurately reflects the natural
465 variations and interconnections present in the subsurface. This consistency is essential for making
466 informed decisions in geological exploration ultimately leading to more reliable outcomes in our
467 geological interpretations.

468 In the proposed correlation algorithm, we can select between summation and multiplication for
469 calculating the correlated score in step iii. Summation is less sensitive to outliers; for instance, if one
470 drillhole in the set has a zero score, using multiplication would result in a total score of zero.
471 Additionally, we can apply weighting to different drillholes, such as by using geological distance, to
472 reduce the influence of more distant drillholes on the overall score.

473 Moreover, it's important to note that the algorithm exhibits linear scalability with respect to the
474 number of drillholes. This efficiency is achieved by utilizing solution connectivity graphs rather than
475 evaluating each pair of solutions individually, which can be computationally expensive.

476 We utilize solution correlation analysis to identify compatible stratigraphic orderings between
477 multiple drillholes, serving as a constraint on the plausibility of individual solutions. This correlation
478 leverages the topological relationships of units represented through local connectivity graphs from
479 each drillhole.

480 A key challenge in correlating stratigraphy logs is that units at the same depth may not align across
481 different drillholes due to variations in unit dip and thickness, tectonic deformation, and stratigraphic
482 gaps (such as unconformities or erosional surfaces). To address this, we focus on correlation based
483 on topological relationships rather than depth-matching. The local connectivity graph G_h for each

485 [drillhole \$h\$ is constructed from the complete set of solutions \$S_h\$, obtained via the Branch and Prune](#)
486 [algorithm \(Section 2.2\), where nodes represent geological units, edges represent stratigraphic](#)
487 [ordering between units, and edge weights \$w_h\(u_i, u_{i+1}\)\$ represent the probability of unit contacts](#)
488 [within that drillhole's solution ensemble.](#)

489 [To facilitate correlation analysis, we generalize the scoring function from Section 2.2 to evaluate any](#)
490 [solution \$s_i\$ against any local connectivity graph. Define the generalized scoring function as:](#)

491
$$\text{score}(s_i, G_h) = \sum_i w_h(u_i, u_{i+1}) / N_i,$$

492 [where the sum is over all consecutive unit pairs \$\(u_i, u_{i+1}\)\$ in solution \$s_i\$. \$G_h\$ represents any local](#)
493 [connectivity graph derived from drillhole solutions, \$w_h\(u_i, u_{i+1}\)\$ denotes the edge weight from graph](#)
494 [\$G_h\$ for that unit pair, and \$N_i\$ is the number of unit contacts in solution \$s_i\$. Note that \$G_h\$ refers to local](#)
495 [connectivity graphs from drillhole solutions, not the global connectivity graph \$\Gamma\$ from map data](#)
496 [\(Section 2.2\). If an edge \$\(u_i, u_{i+1}\)\$ from solution \$s_i\$ does not exist in \$G_h\$, its weight is taken as zero. This](#)
497 [generalized function allows us to assess how consistent a solution from one drillhole is with the](#)
498 [geological relationships observed in other drillholes.](#)

499 **[Correlation Algorithm:](#)**

500 [Consider a set of \$H\$ drillholes \$\{h_1, h_2, \dots, h_H\}\$ with their respective local connectivity graphs \$\{G_1, G_2, \dots, G_H\}\$. For each solution \$s_i\$ from any drillhole, we compute a correlated score that represents the](#)
501 [average consistency across all drillholes:](#)

503
$$\text{scorecorr}(s_i) = (1/H) \sum_{k=1}^H \alpha_k \text{score}(s_i, G_k),$$

504 [where \$\alpha_k\$ are weighting factors that can be based on geological distance \(distance between collar and](#)
505 [closest node of map polygon\), drillhole quality, or other criteria. This equation computes an average](#)
506 [score across all drillholes. The division by \$H\$ ensures the correlated score remains on a comparable](#)
507 [scale regardless of the number of drillholes. In this work, we use \$\alpha_k = 1\$ for all drillholes, giving equal](#)
508 [weight to each drillhole. This summation approach is robust to outliers; if one drillhole yields a zero](#)
509 [score, it does not eliminate the entire correlation. Alternative weighting schemes such as \$\alpha_k = 1/d\(h_i, h_k\)\$](#)
510 [could be employed to reduce the influence of more distant drillholes.](#)

511 [The correlated scores are then normalized to obtain a revised probability distribution:](#)

512
$$P_{\text{corr}}(s_i) = \text{scorecorr}(s_i) / \sum_m \text{scorecorr}(s_m),$$

513 [The correlated probability \$P_{\text{corr}}\(s_i\)\$ provides a revised ranking of solutions that accounts for both](#)
514 [local evidence and regional consistency. Solutions with unit contacts that appear frequently across](#)
515 [multiple drillholes receive higher correlated scores, while solutions unique to a single drillhole](#)
516 [receive lower scores. This correlation effectively reduces uncertainty by leveraging spatial geological](#)
517 [consistency.](#)

518 **[Summation vs. Multiplication:](#)** While the equation for `scorecorr` uses weighted summation, an
519 [alternative multiplicative approach could also be formulated. However, multiplicative forms are more](#)
520 [sensitive to outliers: if any single drillhole yields a zero score, the entire correlated score becomes](#)
521 [zero. Therefore, the summation approach is generally preferred for its robustness.](#)

522 **[Computational Efficiency:](#)** The algorithm achieves $O(H^2 |S|)$ complexity when correlating solutions
523 [across all \$n\$ drillholes. This efficiency is achieved by comparing solutions against pre-computed](#)
524 [connectivity graphs \$G_h\$ rather than individual solutions. The alternative of solution-to-solution](#)
525 [comparison would scale as \$O\(H^2 |S|^2\)\$ and be computationally prohibitive.](#)

526 By integrating and correlating drillhole data through this topological approach, we ensure that the
527 stratigraphic framework accurately reflects the natural spatial variations and interconnections
528 present in the subsurface. The correlation process quantitatively reduces uncertainty by identifying
529 and favoring solutions that are geologically consistent across the broader area. This uncertainty
530 reduction is achieved by concentrating probability mass on solutions supported by multiple drillholes
531 while downweighting locally anomalous interpretations. The resulting correlated probabilities
532 $P_{corr}(s_i)$ provide more reliable stratigraphic interpretations than single-drillhole probabilities $P(s_i)$,
533 enabling more informed decisions in geological exploration and 3D geological modeling.

534

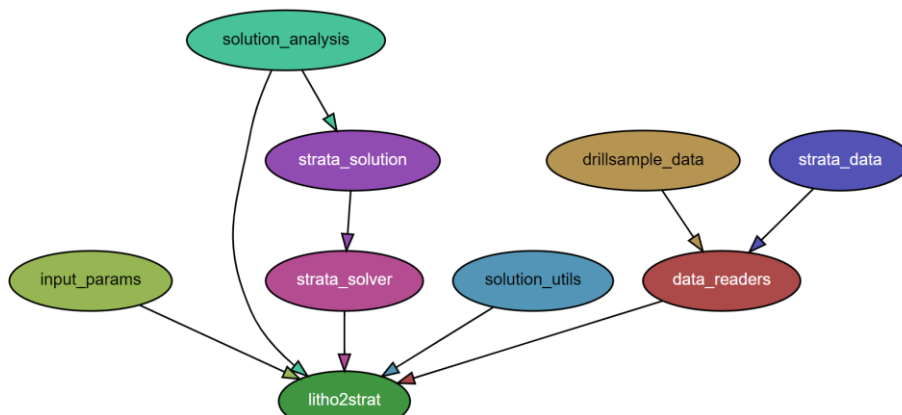
535 [2.6 2.4-Code design](#)

536

537 A Python package called litho2strat has been developed for stratigraphy recovery. It can be easily
538 installed using the command “`pip install`”, and it has minimal external library dependencies: `numpy`,
539 `matplotlib`, and `NetworkX`. The `NetworkX` library is utilized to create a directed graph data structure
540 that represents the topological relationships of relative unit ages (Hagberg et al., 2008). It also
541 supports exporting graphs to `GML` format (Himsolt, 1997) for advanced graph visualization with tools
542 like `yEd` (<https://www.yworks.com/products/yed>).

543 Interaction with the code is facilitated through a *Parfile*, a text file that contains all necessary
544 parameters and paths to the input data files. The parameters in the *Parfile* are organized into several
545 categories based on their functionality, including input file paths, solver settings, and data
546 preprocessing options. An example of such a *Parfile* is provided in Appendix A.

547 The code architecture efficiently organizes distinct modules, including data reader, the user interface
548 (represented by the *Parfile*), the algorithms (such as the solver), and the visualization components
549 (e.g., output figures and graphs), as shown in Fig. 32. This design enhances code readability, making
550 it easier for developers to understand and navigate the codebase. Additionally, it facilitates further
551 extensions by allowing new features to be integrated seamlessly. *This structure also supports*
552 *effective testing, enabling modifications to be verified systematically and reducing the risk of*
553 *introducing errors. The structure also supports effective testing, ensuring that modifications can be*
554 *verified without introducing errors.*



555

Formatted: Outline numbered + Level: 2 + Numbering Style: 1, 2, 3, ... + Start at: 1 + Alignment: Left + Aligned at: 0 cm + Indent at: 0.81 cm

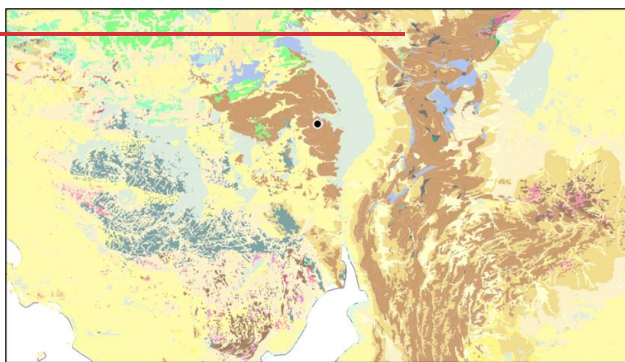
556 Figure 32: The module dependencies of the *litho2strat* code. The graph is generated by the *pydeps*
557 utility, while excluding external dependencies.

558 3. Example Use

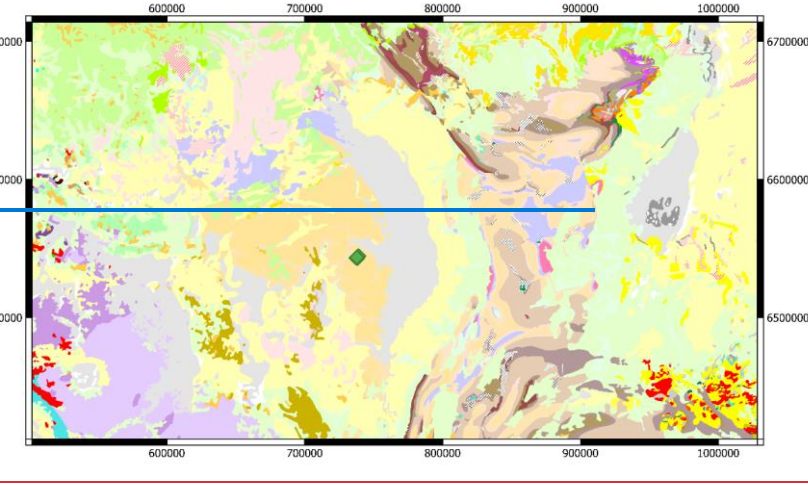
559

560 For this example, we used a set of 52 drillholes from South Australia originally drilled by Teck
561 Cominco Pty. Ltd. (Fig. 43). This area was chosen as there were a number of holes equally spaced
562 with a relatively homogenous spatial distribution and the holes provided both lithological logs and
563 existing interpretations of the down-hole stratigraphy.

564



565



566

567 Figure 43: Location of South Australia test area (drillholes shown as green diamonds), together with
568 an example stratigraphic log, map from 1:2M Surface Geology Map of South Australia (The

569 [Department for Energy and Mining, the Government of South Australia, Geoscientific Data, Sourced
570 on 22 July 2018, \[http://energymining.sa.gov.au/minerals/geoscience/geological_survey/data\]\(http://energymining.sa.gov.au/minerals/geoscience/geological_survey/data\)
571 GDA94/Zone 53\).](http://energymining.sa.gov.au/minerals/geoscience/geological_survey/data)

572 Data Cleaning

573 Examples of terms in the ignore list for this case study include:

Breccia (Undiff. Origin)
Ironstone (Metasomatic)
No Information
Solution-Collapse Breccia
574 Vein (Undifferentiated)

575 Examples of terms in the ignore list for this case study include the following, where each term is
576 excluded from drillhole lithology log processing:

577 1. Breccia (Undiff. Origin)
578 2. Ironstone (Metasomatic)
579 3. No Information
580 4. Solution-Collapse Breccia
581 5. Vein (Undifferentiated)
582 5. Examples of the thesaurus of synonyms for this case study area include:

dolomite, dolomite rock, carbonate rock, limestone
conglomerate, diamictite
grit, sandstone, quartzite, siltstone
gabbro, gabbronorite

583 584 Examples of the thesaurus of synonyms for this case study area include the following groups, where
585 each group contains lithology names that are treated as equivalent:

586 1. dolomite, dolomite rock, carbonate rock, limestone
587 2. conglomerate, diamictite
588 3. grit, sandstone, quartzite, siltstone
589 4. gabbro, gabbronorite

590

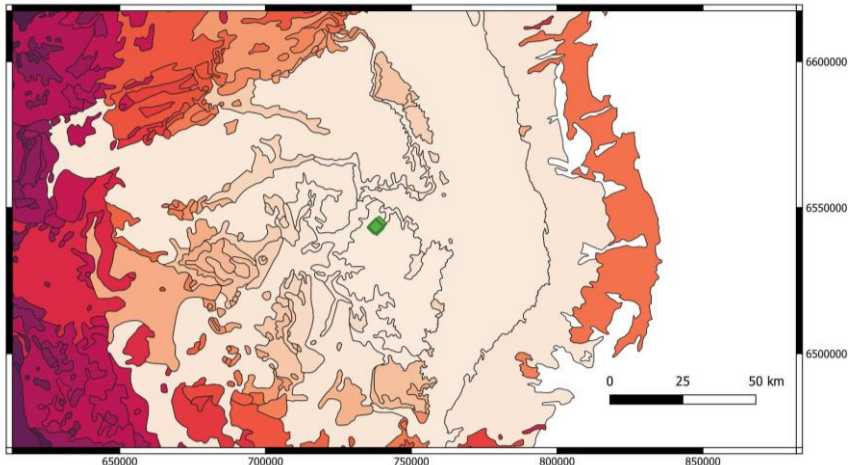
591 Map Analytics

592 The [Figure 5 below](#) shows stratigraphic units coloured as a function of the distance to one of the
593 drillholes ([Fig. 4](#)). A large search area was used for this example as the stratigraphy is fairly flat lying
594 so there is no guarantee that a unit will reach the surface in the local neighbourhood.

Formatted: List Paragraph, Numbered + Level: 1 + Numbering Style: 1, 2, 3, ... + Start at: 1 + Alignment: Left + Aligned at: 0.63 cm + Indent at: 1.27 cm

Formatted: List Paragraph, Numbered + Level: 1 + Numbering Style: 1, 2, 3, ... + Start at: 1 + Alignment: Left + Aligned at: 0.63 cm + Indent at: 1.27 cm

Formatted: List Paragraph, Numbered + Level: 1 + Numbering Style: 1, 2, 3, ... + Start at: 1 + Alignment: Left + Aligned at: 0.63 cm + Indent at: 1.27 cm



595

596 [Figure 54. Distant Distance](#) of stratigraphic units [from](#) [to](#) drillholes (darker [colours](#) signifies larger
597 [distance](#)). Green diamonds show the location of the drillholes [\(Same source map as Fig. 43,](#)
598 [GDA94/Zone 53\)](#).

599 [In the initial analysis we plotted a network graph of all known topological relationships between](#)
600 [stratigraphic units based on the geology map \(extending out 100 km from the test area\), the ASUD](#)
601 [database, and additional information from published reports \(Fig. 5\).](#)

602 [In the initial analysis we constructed the global connectivity graph \$\Gamma\$ \(Section 2.2\), representing](#)
603 [topological relationships between stratigraphic units. The initial graph was constructed automatically](#)
604 [from the geology map \(extending out 100 km from the test area\) using the map2model software, then](#)
605 [manually extended with additional topological relationships from the ASUD database and published](#)
606 [reports. The graph was processed using the NetworkX Python library, exported to GML format, and](#)
607 [visualized using yEd software \(Fig. 6\). The global connectivity graph consists primarily of single-](#)
608 [direction edges, with two bidirectional edges \(Whyalla Sandstone–Angepena Formation and](#)
609 [Paleoproterozoic–Mesoproterozoic Rocks–Donington Suite\) to account for spatial variability in their](#)
610 [stratigraphic relationships.](#)

611

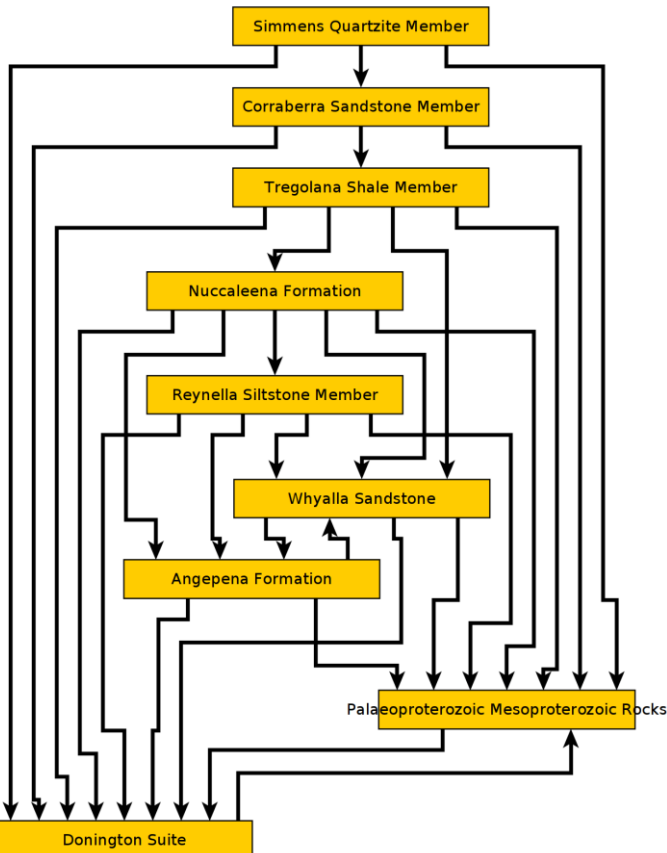


Figure 65: Topological relationships between units in and around the test area.

612

613

614

615

616 Drillhole Analytics

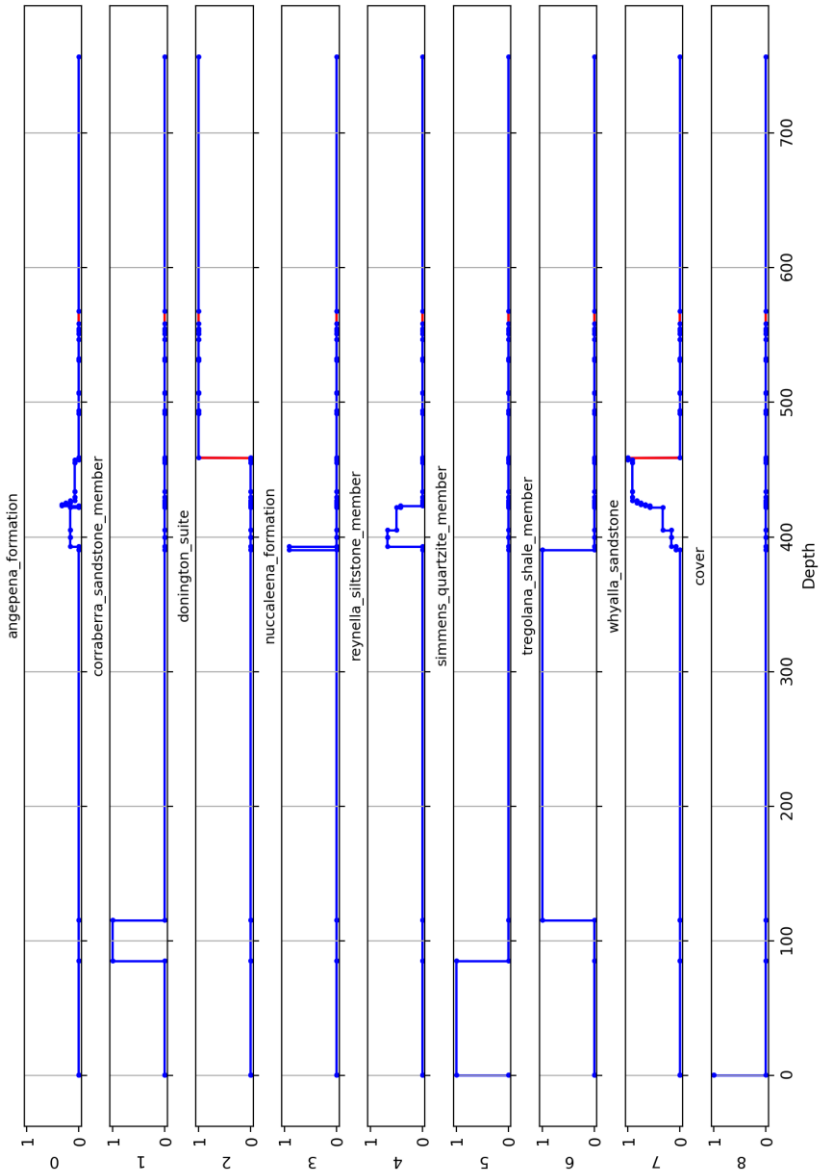
617 The drillholes analysis calculated every possible stratigraphic ordering that was consistent with the
 618 observed lithological ordering down the drillhole and solution constraints (described in Sec. 2.3). By
 619 collating the results for all possible solution paths, we can produce estimates of the marginal
 620 probability that any depth interval will be a particular stratigraphic unit (Fig. 76). For depth interval i
 621 and stratigraphic unit u , the probability $P_{i|u}$ is computed as:

$$622 P_{i|u} = |\{s \in S : s[i] = u\}| / |S|,$$

623 where S is the set of all valid solutions and $s[i]$ denotes the unit assigned to interval i in solution s .

624

Probability of occurrence for every unit. CollarID = 265003

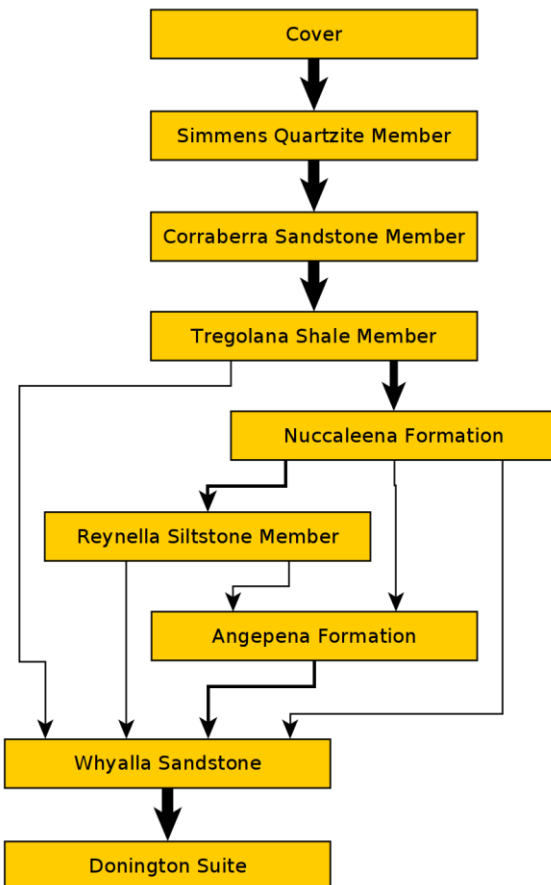


625

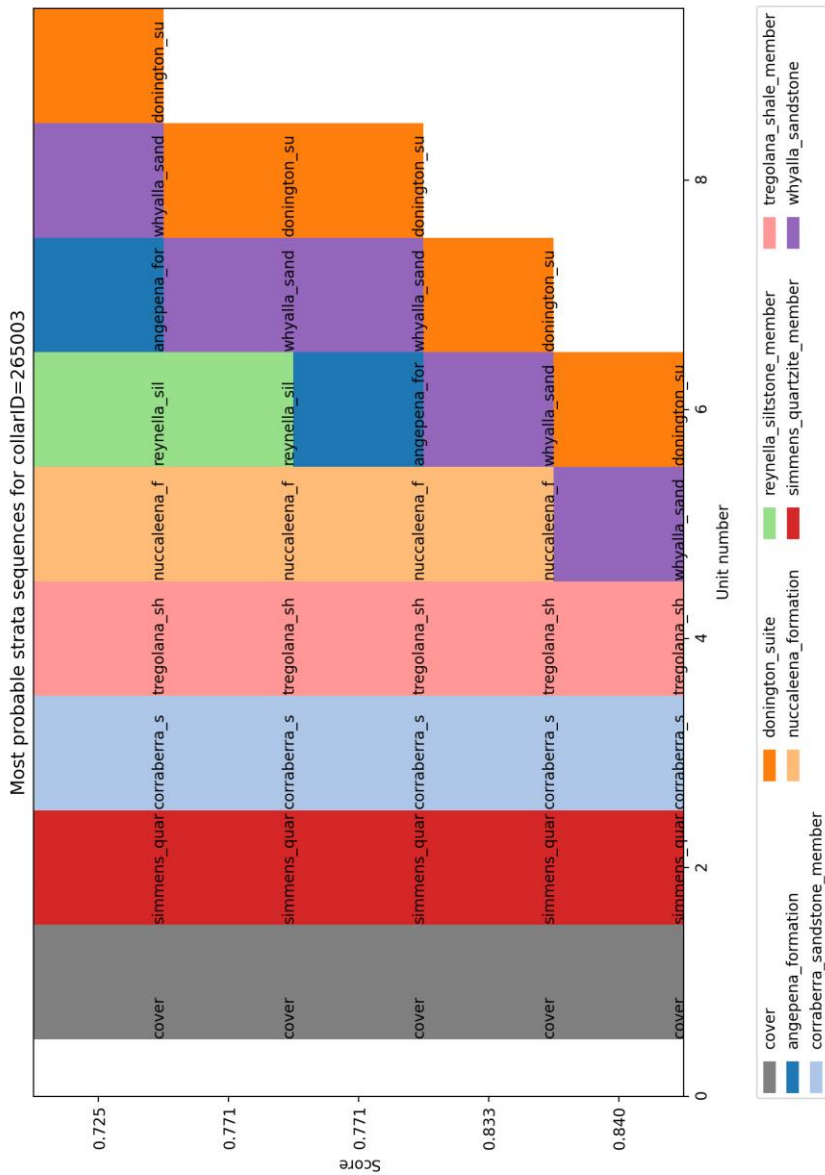
626 Figure 26: Estimated probability of each stratigraphic unit occurring at a given depth for a single
627 drillhole.

628 In Fig. 27, we present the final (local) unit connectivity derived from the stratigraphic solutions
629 generated. The width of the graph edges indicates the probability of unit contacts, with thicker edges

630 signifying higher probabilities. This visual representation allows for a clear comparison of
631 connectivity before (Fig. 6) and after the stratigraphic analysis.



632
633 Figure 87: Calculated local topology using all solutions. Graph edges (relationships) between two
634 stratigraphic units are displayed as a probability of a that contact-relationship occurring.
635 The final solution score for a single ordering is calculated by summing of the probabilities of the
636 contact edge weights. This allows us to sort the orderings by probability, ignoring stratigraphic
637 thickness for now (Fig. 98).

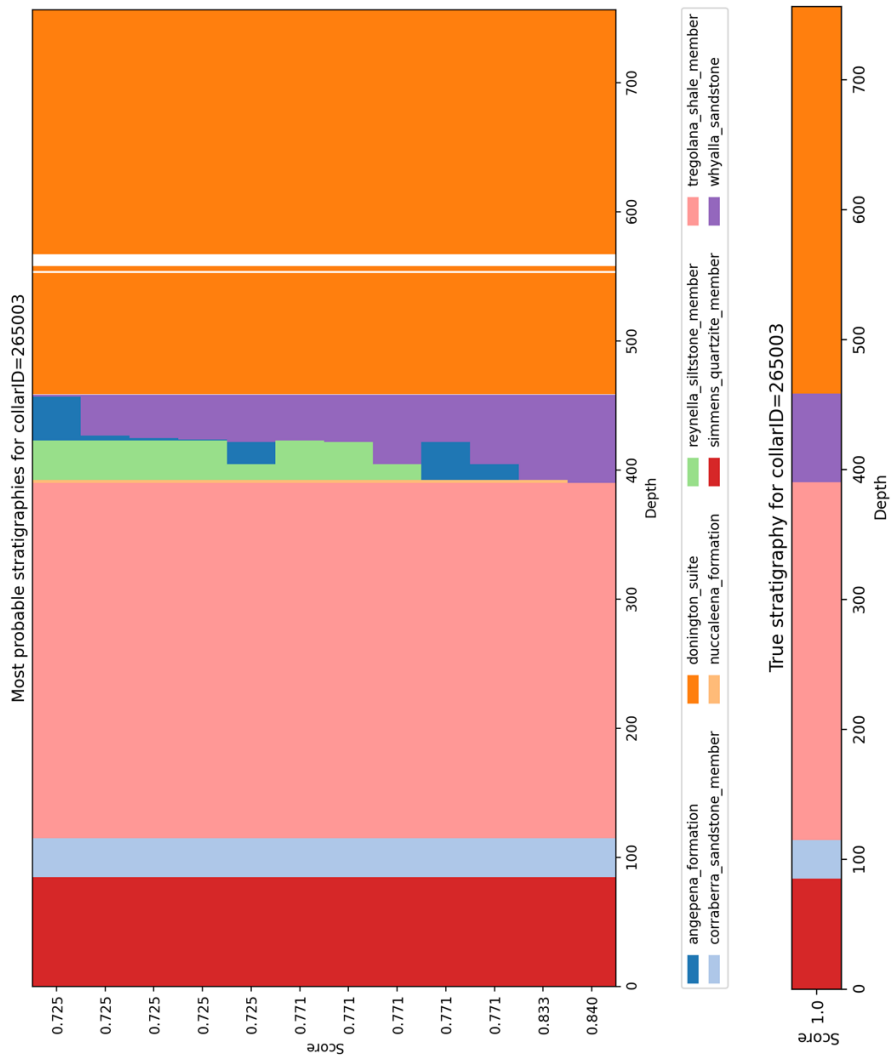


638

| 639 Figure 98: The 5 most probable stratigraphic orderings, with their solution probability on the x axis
640 and order of depth on the y axis.

641

642 Finally, we can then include the depths to contacts between units in the drillhole based on the
643 previous analyses (Fig. [109](#)).



644
645 Figure [109](#): The 12 most probable stratigraphic orderings showing true depth of contact (above)
646 compared to the stratigraphy as logged for the same hole.

647

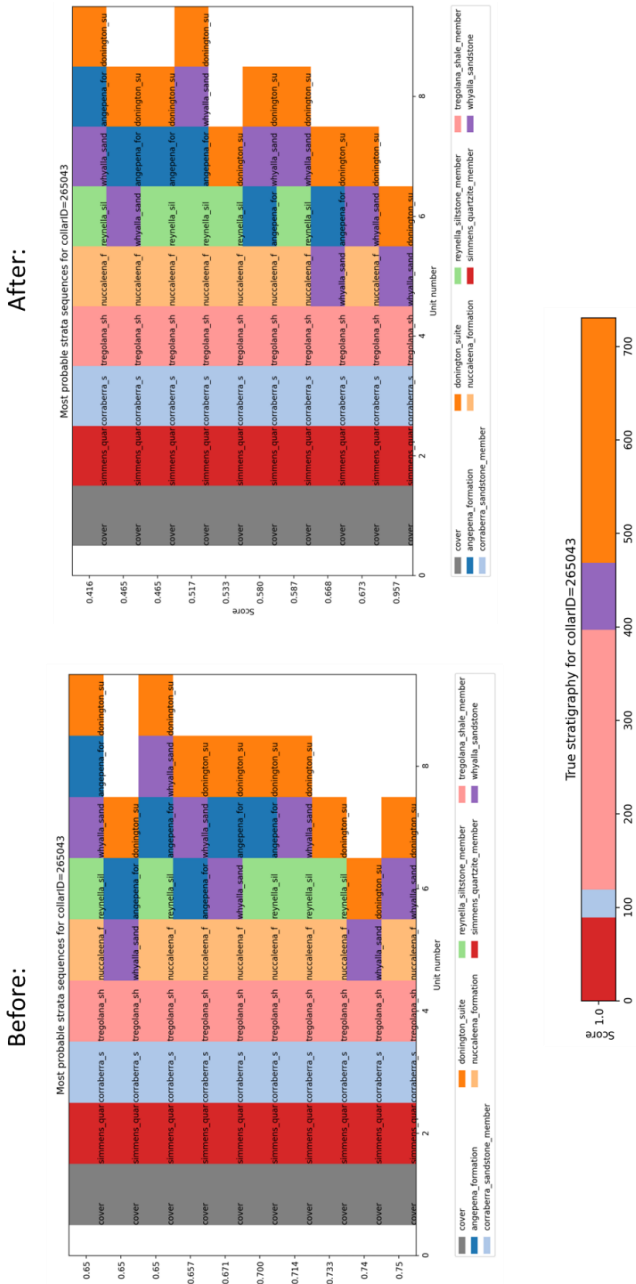


Figure 110: Comparison of ordering for one hole (left) vs ordering for that hole considering the outcomes of 45 other drillholes in the neighbourhood.

651

652 In the next stage of our analysis, we perform solution correlation across multiple drill holes to
653 establish a plausible stratigraphic order and reduce uncertainty. Figure 1¹⁰ illustrates the comparison
654 of the most probable stratigraphies before and after correlation. Prior to correlation, the solution
655 that aligns with the “true” stratigraphy (the correct solution) is ranked second, with a score of
656 $S=0.74$, while the highest-ranked solution has a score of $S=0.75$. However, after applying the
657 correlation, the correct solution rises to the top rank with a score of $S=0.95$, whereas the previously
658 highest-ranked solution falls to second place with a score of $S=0.67$. This correlation analysis not only
659 helped identify the correct solution but also significantly reduced its relative uncertainty, increasing
660 the relative score between the top two solutions from 1% to 42%.

661 [The computational efficiency of the litho2strat algorithm was evaluated through performance testing](#)
662 [on this dataset, with scalability analysis presented in Appendix B.](#)

663

664 4. Discussion and Future Work

665

666 Whilst we were able to develop a workflow that successfully provided useful stratigraphic analyses
667 for our test area, we recognise that for other areas the methodology was not always as successful.
668 We have identified several aspects of the current stratigraphic descriptions that we think will
669 significantly expand the useability of the workflow we present above.

670 1) Lithological Uncertainty. The principal reason for this was that the lithological descriptions of
671 stratigraphies in many areas is quite vague. Successive stratigraphic units in a group might
672 have very similar lithological descriptions.

673 As an example, we look at the Hamersley Group, in Western Australia (Maldonado & Mercer,
674 2018). If we examine the GSWA explanatory notes for three successive formations (Mt McRae
675 Shale, Mt Sylvia Formation and the Wittenoom Formation) in the GSWA explanatory notes
676 their lithologies are described as:

- 677 • **Mt McRae Shale** - Mudstone, siltstone, chert, iron-formation, and dolomite. Thin
678 bands of shard-bearing volcanic ash in upper parts.
- 679 • **Mt Sylvia Formation** - Mudstone, siltstone, chert, iron-formation, and dolomite.
- 680 • **Wittenoom Formation** - Thinly bedded dolomite and dolomitic shale, with minor
681 black chert, shale, banded iron formation and sandstone.
- 682 •

683 Formatted: List Paragraph, Bulleted + Level: 1 +
684 Aligned at: 1.9 cm + Indent at: 2.54 cm

683 We can see that there is a significant overlap in lithologies, with an ordering of lithologies but
684 without constraints on the percentage of each lithology in the three formations. This
685 additional information, even as an estimate, would provide useful constraints on the likelihood
686 that a specific lithology is associated with a given stratigraphic unit.

687

688 2) Min-Max thickness estimates. In some areas, there is useful information on the minimum,
689 maximum and average stratigraphic thickness of units.

691 3) Stratigraphic ordering of lithologies. Additional information on commonly occurring orderings
692 of lithologies within a given formation or member would also provide useful constraints.
693

West Angela Member

Derivation of name/Formal lithostratigraphy

The West Angela Member was the first subdivision of the Wittenoom Formation to be formally recognized (Blockley et al., 1993). It is named after West Angela Hill (Zone 50, MGA 673387E 742407N) near the West Angels iron ore mine, and the type section is defined as the interval between 420.4 m and 524.6 m in drill hole WRL 1 (Blockley et al., 1993) stored at the Geological Survey of Western Australia (GSWA) Carlisle Core Library.

Five shaly horizons separated by BIF, chert, or massive dolomite are recognized in the West Angela Member and are informally designated as AS1 to AS5 (Kepert, 2018). In particular the lower three shale horizons form a distinctive pattern in natural gamma-ray logs that can be used for regional correlation (Blockley et al., 1993).

Minimum thickness(m) —
Maximum thickness(m) 80

Lithology

The West Angela Member is generally not well-exposed and consists predominantly of dolomite and shaly dolomite, with minor chert, BIF, volcaniclastic rocks, and impact ejecta layers. Near the base, there is a distinctive unit of interbedded chert, BIF, dolomitic shale, and shale with characteristic natural gamma-ray peaks that are designated AS1 to AS3 (Blockley et al., 1993). This entire interval is referred to as A1 by some mining companies (e.g. Kepert, 2018) and is overlain by a thick interval of shale and dolomitic shale (AS3). The middle of the member, between AS3 and AS 4, contains a unit of massive to laminated crystalline dolomite with local carbonaceous shale and siltstone partings (Blockley et al., 1993). The upper part of the West Angela Member (AS4 to AS5) consists mainly of dolomitic shale and shale with minor chert beds that is gradationally overlain by massive dolomite at the base of the Paraburadoo Member. Lateral correlations between drillholes WRL 1 and FVG 1 suggest that the member becomes shaler towards the east (Blockley et al., 1993).

694
695 Figure 124: Free-text descriptions of the West Angela Member in the GSWA Explanatory Notes.
696
697
698
699
700
701
702
703

All three of these types of information are often included in the free-text portions of stratigraphic databases, such as the example shown for the West Angela Member in the GSWA Explanatory Notes in Fig. 124. In this example the free-text provides more specific information on the thickness, the ordering of lithologies and the relative proportions of lithologies. With the advent of more sophisticated Machine Learning methodologies, the extraction of this ancillary data in a standardised form from reports and the stratigraphic databases themselves will open up new possibilities for constraining stratigraphy. Similarly, the codes developed in dh2loop for harmonising lithological terminologies will expand greatly in coming years.

704 4) Inclusion of discontinuity information in the litho2strat workflow (most often logged faults)
705 could help to define where breaks in stratigraphy are most likely to occur
706
707 5) Inclusion of secondary descriptive information (for example grain size) could help to refine our
708 younging estimators in areas of uncertain facies.
709
710 6) There is no doubt that the advent of Large Language Models will have a profound effect on
711 our ability to extract and categorize information from unstructured data sources, and
712 algorithms based on these approaches will probably replace the data extraction and data
713 harmonisation modules in future versions of this workflow.

716

717 5. Conclusions

718

719 We developed codes and methodologies for stratigraphy recovery from drillhole databases, utilizing
720 the branch and [bound-prune](#) algorithm as a foundational framework. To ensure the generation of
721 geologically plausible solutions, we implemented various types of constraints that account for the
722 complexities of subsurface geology.

723 To further reduce uncertainty in the obtained solutions, we introduced a correlation algorithm that
724 leverages information from multiple drillholes simultaneously. This innovative approach allows for a
725 more robust analysis by integrating data across different locations, enhancing the reliability of the
726 stratigraphic interpretations.

727 Our proposed method was applied to a dataset comprising 52 drillholes from South Australia. The
728 results demonstrated that the algorithm successfully predicts the correct stratigraphic solution while
729 providing associated uncertainty metrics, effectively validating its performance against measured
730 stratigraphy data.

731 Additionally, we identified several key aspects of the current stratigraphic descriptions that could
732 significantly enhance the usability of the workflow we have presented. These enhancements aim to
733 improve the accessibility and applicability of our methodology, paving the way for more effective
734 geological assessments and decision-making processes in the field.

735

736

737

738

739

740

741

742

743

744

745

746

747

748

749

750

751

752 *Code and data availability.* The software and datasets used in this study are publicly available for
753 download at GitHub (<https://github.com/Loop3D/litho2strat>) and Zenodo
754 (<https://doi.org/10.5281/zenodo.15064469>, Ogarko et al., 2025).

755 *Author contribution.* VO and MJ are the primary contributors to this study. VO led the research,
756 developed the methodology and software, and prepared the manuscript. MJ provided guidance on
757 drillhole data analysis and contributed to manuscript writing.

758 *Competing interests.* The authors declare that they have no conflict of interest.

759 *Acknowledgements.* The work has been supported by the Mineral Exploration Cooperative Research
760 Centre whose activities are funded by the Australian Government's Cooperative Research Centre
761 Program. This is MinEx CRC Document [20**/**2025/27](#). We are grateful to reviewer Guillaume
762 [Caumon for very helpful comments that greatly improved the paper.](#)

Formatted: Font: (Default) +Body (Calibri)

763 Appendix A- Control file for litho2strat code

764

765 Example usage: `python3 litho2strat.py -p ./parfiles/Parfile_SA.txt`

766

767 Example parfile:

```
[FilePaths]
topology_filename = data/SA_test_data/newpairs_20_06_2023.gml
cover_unit_filename =
ignore_list_filename = data/SA_test_data/ignore_list.txt
alternative_rock_names_filename = data/SA_test_data/alternative_rock_names.txt
unit_colors_filename = data/SA_test_data/unit_colors.csv
drillsample_filename = data/SA_test_data/litho_tables/litho_$collarID$.csv
stratasample_filename = data/SA_test_data/strat_tables/strat_$collarID$.csv
dist_table_filename = data/SA_test_data/dh_asud_strat2.csv

[DataHeaders]
drillsample_header = DEPTH_FROM_M, DEPTH_TO_M, MAJOR_LITHOLOGY,
stratasample_header = DEPTH_FROM_M, DEPTH_TO_M, STRAT_UNIT_NAME,
strata_data_header = strat, summary, distance, description

[SolverParameters]
add_topology_constraints = True
max_num_strata_jumps = 0
max_num_returns_per_unit = 0
max_num_unit_contacts_inside_litho = 0
single_top_unit = True

[Correlation]
correlation_power = 1.0

[DataPreprocessing]
number_nearest_units = 10
min_drillhole_litho_score = 80
group_drillhole_lithos = False
cover_ratio_threshold = 0.65

[CollarIDs]
collarIDs = 265003,265010,265018,265030,265043,265051
```

768

769

770

771

772

773

774

Formatted: Font color: Auto

Formatted: Normal

Formatted: Left

```

775 [FilePaths]
776 topology filename = data/SA_test_data/newpairs_20_06_2023.gml
777 ignore_list filename = data/SA_test_data/ignore_list.txt
778 alternative_rock_names filename = data/SA_test_data/alternative_rock_names.txt
779 unit_colors filename = data/SA_test_data/unit_colors.csv
780
781 drillsample filename = data/SA_test_data/litho_tables/litho_$collarID$.csv
782 stratasample filename = data/SA_test_data/strat_tables/strat_$collarID$.csv
783 dist_table filename = data/SA_test_data/dh_asud_strat2.csv
784
785 [DataHeaders]
786 drillsample header = DEPTH_FROM_M, DEPTH_TO_M, MAJOR_LITHOLOGY,
787 stratasample header = DEPTH_FROM_M, DEPTH_TO_M, STRAT_UNIT_NAME,
788 strata_data header = strat, summary, distance, description
789
790 [SolverParameters]
791 add_topology_constraints = True
792 max_num_strata_jumps = 0
793 max_num_returns_per_unit = 0
794 max_num_unit_contacts_inside_litho = 0
795 single_top_unit = True
796
797 [DataPreprocessing]
798 number_nearest_units = 10
799 min_drillhole_litho_score = 80
800 group_drillhole_lithos = False
801 cover_ratio_threshold = 0.65
802
803 [CollarIDs]
804 collarIDs = 205821,205822,264999,265000,265001

```

← **Formatted:** Left, Indent: Left: 1.27 cm, Space After: 0 pt, Line spacing: single

← **Formatted:** Indent: Left: 1.27 cm, Space After: 0 pt, Line spacing: single

← **Formatted:** Left, Indent: Left: 1.27 cm, Space After: 0 pt, Line spacing: single

805 Appendix B: Performance and Scalability Analysis

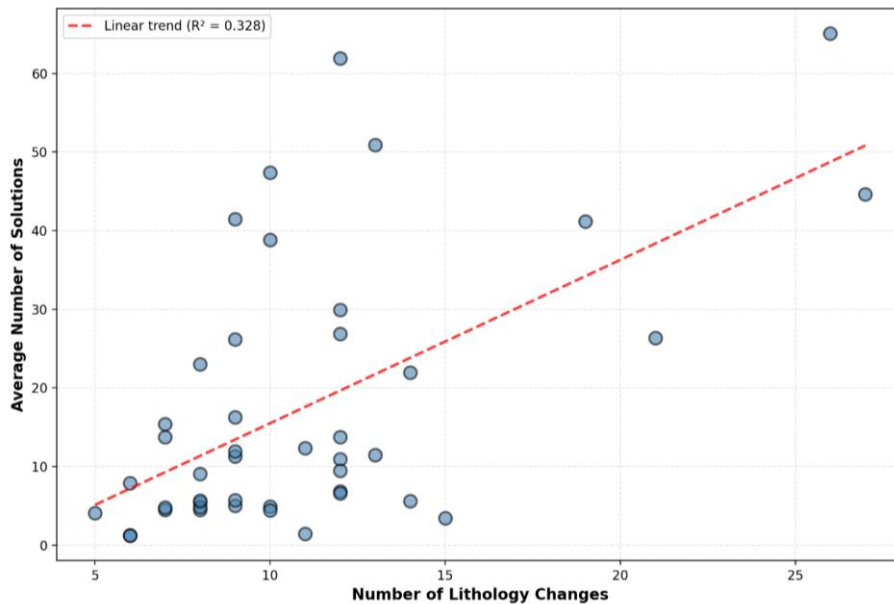
Formatted: Font: Not Bold

Formatted: Left

807 To complement the theoretical complexity analysis presented in Section 2.4, we conducted empirical
808 tests to evaluate the performance and scalability of the litho2strat algorithm. We tested how the
809 average number of solutions maintained during recursive exploration (N) scales with the number of
810 lithology changes in drillhole logs, comparing two scenarios: (1) using the global topology graph Γ as
811 a constraint, and (2) without topology constraints.

812 Figure B.1 shows the relationship between the number of lithology changes and the average number
813 of solutions maintained during recursive exploration when the topology graph constraint is applied.
814 The results demonstrate near-linear scaling, confirming that the topology graph effectively prunes
815 the solution space while preserving geological validity.

816

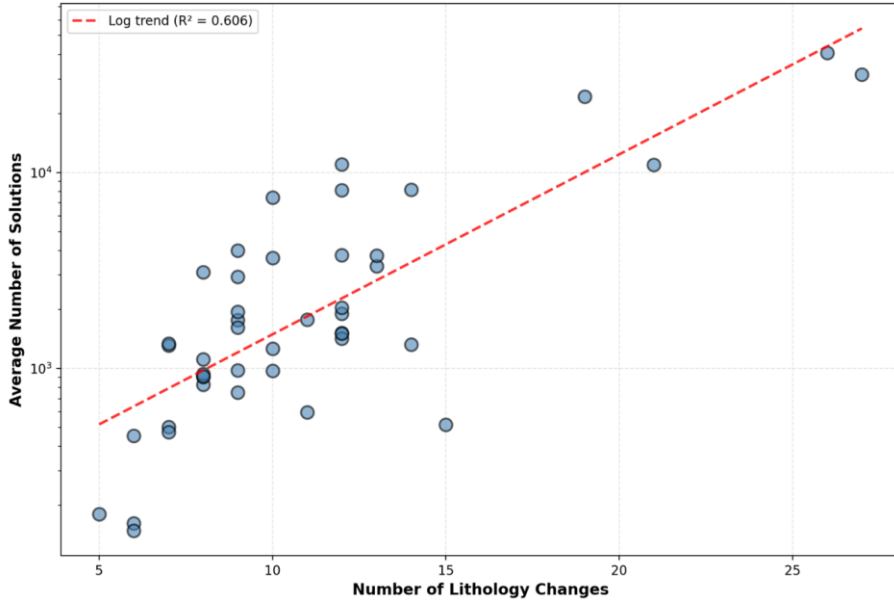


817

818 Figure B.1: Average number of solutions maintained during recursive exploration versus number of
819 lithology changes with topology graph constraint.

Formatted: Left

820 Figure B.2 presents the same relationship for the unconstrained case, where the algorithm considers
821 all theoretically possible stratigraphic interpretations. Here, the average number of solutions
822 maintained during recursive exploration exhibits near-exponential growth with increasing lithology
823 changes, illustrating the combinatorial explosion that occurs without geological constraints.



824

825 [Figure B.2: Average number of solutions maintained during recursive exploration versus number of](#)
 826 [lithology changes without topology constraints.](#)

827 [The computational performance measurements further highlight the practical importance of these](#)
 828 [constraints. Using a single CPU core \(Intel i7-1185G7 @ 3.00GHz\) to process all 52 drillholes from](#)
 829 [Section 3 and perform the correlation of solutions, the constrained approach required approximately](#)
 830 [1 second total processing time, while the unconstrained case required approximately 50 seconds for](#)
 831 [the same dataset. This 50-fold improvement in computational efficiency, combined with the near-](#)
 832 [linear versus near-exponential scaling behavior of solutions maintained during recursive exploration,](#)
 833 [demonstrates that incorporating geological knowledge through the topology graph is essential for](#)
 834 [both computational tractability and practical applicability of the litho2strat algorithm to real-world](#)
 835 [geological datasets.](#)

836

837

838

839

840

841

842

843

844

Formatted: Left

845

846 Alvarado-Neves, F., Ailleres, L., Grose, L., Cruden, A. R., & Armit, R. (2024). Three-dimensional
847 geological modelling of igneous intrusions in LoopStructural v1.5.10. *Geoscientific Model
848 Development*, 17(5), 1975–1993. <https://doi.org/10.5194/gmd-17-1975-2024>

849 Calcagno, P., Chilès, J. P., Courrioux, G., & Guillen, A. (2008). Geological modelling from field data and
850 geological knowledge. *Physics of the Earth and Planetary Interiors*, 171(1–4), 147–157.
851 <https://doi.org/10.1016/j.pepi.2008.06.013>

852 Caumon, G., Collon-Drouaillet, P., Le Carlier de Veslud, C., Viseur, S., & Sausse, J. (2009). Surface-
853 Based 3D Modeling of Geological Structures. *Mathematical Geosciences*, 41(8), 927–945.
854 <https://doi.org/10.1007/s11004-009-9244-2>

855 D’Affonseca, F. M., Finkel, M., & Cirpka, O. A. (2020). Combining implicit geological modeling, field
856 surveys, and hydrogeological modeling to describe groundwater flow in a karst aquifer.
857 *Hydrogeology Journal*, 28(8), 2779–2802. <https://doi.org/10.1007/s10040-020-02220-z>

858 [Fullagar, P.K., Zhou, B., and Biggs, M., 2004. Stratigraphically consistent autointerpretation of
859 borehole data. Journal of Applied Geophysics, 55\(1-2\), 91-104.
860 https://doi.org/10.1016/j.jappgeo.2003.06.010](#)

861 Giraud, J., Pakyuz-Charrier, E., Jessell, M., Lindsay, M., Martin, R., & Ogarko, V. (2017). Uncertainty
862 reduction through geologically conditioned petrophysical constraints in joint inversion.
863 *GEOPHYSICS*, 82(6), ID19–ID34. <https://doi.org/10.1190/geo2016-0615.1>

864 Guo, J., Wang, Z., Li, C., Li, F., Jessell, M. W., Wu, L., & Wang, J. (2022). Multiple-Point Geostatistics-
865 Based Three-Dimensional Automatic Geological Modeling and Uncertainty Analysis for
866 Borehole Data. *Natural Resources Research*, 31(5), 2347–2367.
867 <https://doi.org/10.1007/s11053-022-10071-6>

868 Guo, J., Xu, X., Wang, L., Wang, X., Wu, L., Jessell, M., Ogarko, V., Liu, Z., & Zheng, Y. (2024). GeoPDNN
869 1.0: a semi-supervised deep learning neural network using pseudo-labels for three-dimensional
870 shallow strata modelling and uncertainty analysis in urban areas from borehole data.
871 *Geoscientific Model Development*, 17(3), 957–973. <https://doi.org/10.5194/gmd-17-957-2024>

872 Hagberg, A. A., Schult, D. A., & Swart, P. J. (2008). *Exploring Network Structure, Dynamics, and
873 Function using NetworkX*. 11–15. <https://doi.org/10.25080/TCWV9851>

874 Hartmann, J., & Moosdorf, N. (2012). The new global lithological map database GLiM: A
875 representation of rock properties at the Earth surface. *Geochemistry, Geophysics, Geosystems*,
876 13(12). <https://doi.org/10.1029/2012GC004370>

877 [Hill, E.J., Pearce, M.A. & Stromberg, J.M. Improving Automated Geological Logging of Drill Holes by
878 Incorporating Multiscale Spatial Methods. *Math Geosci* 53, 21–53 \(2021\).
879 https://doi.org/10.1007/s11004-020-09859-0](#)

880 Himsolt, M. (1997). *GML: a portable graph file format*.

881 Jessell, M. (2001). Three-dimensional geological modelling of potential-field data. *Computers &
882 Geosciences*, 27(4), 455–465. [https://doi.org/10.1016/S0098-3004\(00\)00142-4](https://doi.org/10.1016/S0098-3004(00)00142-4)

883 Jessell, M., Aillères, L., Kemp, E. de, Lindsay, M., Wellmann, F., Hillier, M., Laurent, G., Carmichael, T.,
884 & Martin, R. (2014). Next Generation Three-Dimensional Geologic Modeling and Inversion. In

Formatted: French (France)

Formatted: Font: Not Bold

Formatted: Font: Not Bold

885 *Building Exploration Capability for the 21st Century*. Society of Economic Geologists.
886 <https://doi.org/10.5382/SP.18.13>

887 Jessell, M., Ogarko, V., de Rose, Y., Lindsay, M., Joshi, R., Piechocka, A., Grose, L., de la Varga, M.,
888 Ailleres, L., & Pirot, G. (2021). Automated geological map deconstruction for 3D model
889 construction using <math>map2loop</math> 1.0 and
890 <math>map2model</math> 1.0. *Geoscientific Model Development*,
891 14(8), 5063–5092. <https://doi.org/10.5194/gmd-14-5063-2021> Formatted: French (France)

892 Jessell, M. W., Ailleres, L., & de Kemp, E. A. (2010). Towards an integrated inversion of geoscientific
893 data: What price of geology? *Tectonophysics*, 490(3–4), 294–306.
894 <https://doi.org/10.1016/j.tecto.2010.05.020> Formatted: French (France)

895 Joshi, R., Madaiah, K., Jessell, M., Lindsay, M., & Pirot, G. (2021).
896 <math>dh2loop</math> 1.0: an open-source Python library for
897 automated processing and classification of geological logs. *Geoscientific Model Development*,
898 14(11), 6711–6740. <https://doi.org/10.5194/gmd-14-6711-2021>

899 Land, A. H., & Doig, A. G. (1960). An Automatic Method of Solving Discrete Programming Problems.
900 *Econometrica*, 28(3), 497. <https://doi.org/10.2307/1910129>

901 Lindsay, M. D., Jessell, M. W., Ailleres, L., Perrouty, S., de Kemp, E., & Betts, P. G. (2013). Geodiversity:
902 Exploration of 3D geological model space. *Tectonophysics*, 594, 27–37.
903 <https://doi.org/10.1016/j.tecto.2013.03.013>

904 Maldonado, A., & Mercer, K. (2018). *Comparison of the Laboratory and Barton-Bandis Derived Shear
905 Strength of Bedding Partings in Fresh Shales of the Pilbara, Western Australia. All Days*, ISRM-
906 ARMS10-2018-204.

907 Mallet, J.-L. L. (2002). *Geomodeling*. Oxford University Press, Inc.

908 Martin, R., Ogarko, V., Giraud, J., Plazolles, B., Angrand, P., Rousse, S., & Macouin, M. (2024). Gravity
909 data inversion of the Pyrenees range using Taguchi sensitivity analysis and ADMM bound
910 constraints based on seismic data. *Geophysical Journal International*, 240(1), 829–858.
911 <https://doi.org/10.1093/gji/ggae410>

912 Ogarko, V., Giraud, J., Martin, R., & Jessell, M. (2021). Disjoint interval bound constraints using the
913 alternating direction method of multipliers for geologically constrained inversion: Application to
914 gravity data. *GEOPHYSICS*, 86(2), G1–G11. <https://doi.org/10.1190/geo2019-0633.1>

915 Ogarko, V., & Jessell, M. (2025). litho2strat 1.0 source code,
916 <https://doi.org/10.5281/zenodo.15064469>

917 Pakyuz-Charrier, E., Giraud, J., Ogarko, V., Lindsay, M., & Jessell, M. (2018). Drillhole uncertainty
918 propagation for three-dimensional geological modeling using Monte Carlo. *Tectonophysics*,
919 747–748, 16–39. <https://doi.org/10.1016/j.tecto.2018.09.005>

920 Schetselaar, E. M., & Lemieux, D. (2012). A drill hole query algorithm for extracting lithostratigraphic
921 contacts in support of 3D geologic modelling in crystalline basement. *Computers & Geosciences*,
922 44, 146–155. <https://doi.org/10.1016/j.cageo.2011.10.015> Formatted: French (France)

923 Silversides, K., Melkumyan, A., Wyman, D.A., and Hatherly, P. 2015. Automated recognition of
924 stratigraphic marker shales from geophysical logs in iron ore deposits. *Computers &
925 Geosciences*, 77, 118-125. <https://doi.org/10.1016/j.cageo.2015.02.002>

926 Tarantola, A. (2005). *Inverse Problem Theory and Methods for Model Parameter Estimation*. Society
927 for Industrial and Applied Mathematics. <https://doi.org/10.1137/1.9780898717921>

928 Vollgger, S. A., Cruden, A. R., Ailleres, L., & Cowan, E. J. (2015). Regional dome evolution and its
929 control on ore-grade distribution: Insights from 3D implicit modelling of the Navachab gold
930 deposit, Namibia. *Ore Geology Reviews*, 69, 268–284.
931 <https://doi.org/10.1016/j.oregeorev.2015.02.020>

932 Wedge, D., Hartley, O., McMickan, A., Green, T., and Holden, E., 2019. Machine learning assisted
933 geological interpretation of drillhole data: Examples from the Pilbara Region, Western Australia.
934 Ore Geology Reviews, 114, 103118. <https://doi.org/10.1016/j.oregeorev.2019.103118>

935 Wellmann, F., & Caumon, G. (2018). *3-D Structural geological models: Concepts, methods, and*
936 *uncertainties* (pp. 1–121). <https://doi.org/10.1016/bs.agph.2018.09.001>

937 Wu, X., and Nyland, E., (1987). Automated stratigraphic interpretation of well-log data. Geophysics,
938 52(12), 1665-1676. https://doi.org/10.1190/1.1442283